Published in final edited form as:
J Biomed Mater Res A. 2012 August ; 100(8): 2194–2203. doi:10.1002/jbm.a.34092.

Mass transfer trends occurring in engineered *ex vivo* tissue scaffolds

Marc Moore[1], **Malisa Sarntinoranont**[2], and **Peter McFetridge**[1]

[1]J. Crayton Pruitt Family Department of Biomedical Engineering, University of Florida, JG-56 Biomedical Sciences Building|P.O. Box 116131, Gainesville, Florida 32611-6131

[2]Department of Mechanical and Aerospace Engineering, University of Florida, 212 MAE-A|P.O. Box 116250, Gainesville, Florida 32611-6250

Abstract

In vivo the vasculature provides an effective delivery system for cellular nutrients; however, artificial scaffolds have no such mechanism, and the ensuing limitations in mass transfer result in limited regeneration. In these investigations, the regional mass transfer properties that occur through a model scaffold derived from the human umbilical vein (HUV) were assessed. Our aim was to define the heterogeneous behavior associated with these regional variations, and to establish if different decellularization technologies can modulate transport conditions to improve microenvironmental conditions that enhance cell integration. The effect of three decellularization methods [Triton X-100 (TX100), sodium dodecyl sulfate (SDS), and acetone/ethanol (ACE/EtOH)] on mass transfer, cellular migration, proliferation, and metabolic activity were assessed. Results show that regional variation in tissue structure and composition significantly affects both mass transfer and cell function. ACE/EtOH decellularization was shown to increase albumin mass flux through the intima and proximate-medial region (0–250 μm) when compared with sections decellularized with TX100 or SDS; although, mass flux remained constant over all regions of the full tissue thickness when using TX100. Scaffolds decellularized with TX100 were shown to promote cell migration up to 146% further relative to SDS decellularized samples. These results show that depending on scaffold derivation and expectations for cellular integration, specificities of the decellularization chemistry affect the scaffold molecular architecture resulting in variable effects on mass transfer and cellular response.

Keywords

mass transfer; decellularization; *ex vivo* tissue scaffold; cell migration; diffusion

INTRODUCTION

Molecular architecture of decellularized tissue scaffolds is important, because it directly affects the diffusion of nutrients to and from cells seeded within the extracellular matrix. *Ex vivo* tissue implants must be decellularized to reduce immune complications; however, the harsh surfactants and solvents used for this process alter the ECM and its molecular architecture.[1,2] While some degree of modification is unavoidable, as the process aims to remove soluble components and will by default modify the structural ECM, the extent of alteration is dependent on the approach of the decellularization process. Inherently, mass

Correspondence to: P. McFetridge; pmcfetridge@bme.ufl.edu.

transfer through heterogeneous native tissues is complex, and the decellularization process further complicates diffusion kinetics. Development of *ex vivo*-derived tissue implants requires an understanding of the physical barriers and other tissue specific mass transfer limitations to optimize conditions such as decellularization and nutrient delivery to improve cellular integration and function.[3]

The specificities of the decellularization process are complex and have effects on the scaffold molecular architecture resulting in variable effects on mass transfer and cellular response.[4,5] Many current studies have shown that cell migration is limited to ~200 microns in most tissue scaffolds, with inadequate mass flux of nutrients, wastes, growth factors, and other signaling molecules shown to be the limiting factor in full thickness tissue regeneration.[6] Thus, a more comprehensive understanding of the mass flux kinetics and ECM alterations resulting from both decellularization and natural scaffold architecture is essential.

Cell response to the scaffold environment is dependent on many factors, including pressure, scaffold architecture, growth factors, and scaffold composition.[7–9] In addition, the cell type seeded onto a scaffold will influence its probability to become cell dense because some cell types may be more suited for one particular scaffold composition over another.[10] Besides changes in scaffold architecture and composition, the decellularization process can lead to changes in cell response, which if understood can aid in forming cell dense tissue scaffolds.

Aside from the compositional changes brought about by decellularization, the removal of extracellular matrix proteins, lipids, and sugars also alleviates the physical obstructions which impede nutrients from arriving at the cell surface.[1] While arterial endothelial cells are directly exposed to nutrient rich solutions, cells more distant from the blood interface encounter mass flux limitations such as the extracellular matrix and the endothelial cell layer, which acts as a barrier prior to diffusion toward inner layer cells. Architectural features affecting mass flux include scaffold tortuosity, pore size, scaffold charge, and pore shape.[3] Scaffold architecture has been also shown to have a significant impact on oxygen gradients within forming tissue.[11] As such, scaffold architecture changes resulting from decellularization will have a significant effect on the mass flux rates of other molecules.

The goal of these investigations was to understand further the mass transfer properties of key nutrients through a model *ex vivo* derived vascular scaffold, namely the human umbilical vein (HUV). These data are important in our understanding of critical transfer conditions that modulate cell function to help design improved materials. The HUV was chosen because it shares architectural and structural components such as a tightly woven intimal region and an adjacent less tightly woven layer of collagen that are common to other *ex vivo* scaffolds.[12–14] In addition, if mass transfer conditions of the HUV can be optimized to provide adequate nutrient delivery during early implantation, then it has immense clinical potential as a tissue engineering scaffold.[15]

The HUV was decellularized using three different methods with distinct chemistries: (1) a nonionic surfactant, (2) an ionic surfactant, and (3) a combination of organic solvents and alcohol with acetone/ethanol (ACE/EtOH) as a solubilizing agent. Each method alters the composition and architecture of the scaffold in a different way. Sodium dodecyl sulfate (SDS) is an ionic surfactant that tends to disrupt protein-protein interactions, and solubilizes nuclear remnants and cytoplasmic proteins.[1,16] ACE/EtOH decellularization methods cause protein denaturation, cell lysis, lipid solubilization, and dehydration. This method also leads to a degree of collagen fiber crosslinking.[1,17,18] By comparison, Triton X-100 (TX100) is a nonionic detergent that disrupts lipid-lipid and lipid-protein interactions of cells while

leaving protein-protein interactions intact. TX100 has also been shown to extract near total glycosaminoglycan content as well as decreasing laminin and fibronectin content.[1,16]

In addition to the decellularization by each of these three solutions, a modified mechanical dissection technique was used to isolate different zones of the vascular scaffold (1) the intima and proximate media region, (2) the medial and adventitial regions, and (3) a full-thickness region. Using albumin as a marker molecule, we quantified the mass flux through each zone to understand the relative mass transfer barrier that each region presents (Fig. 1). Our hypothesis was that regional differences in mass transfer would be associated with each of the layers due to variation in the molecular components and architecture of this heterogeneous material. For example, basement membranes typically contain tightly woven type IV collagen, glycoproteins, and heparin sulfate proteoglycans.[19] By comparison, the adventitial region contains mostly loose connective tissue and is surrounded by Wharton's jelly, whose principal components are hyaluronic acid, low-solubility type III collagen.[20] Furthermore, the medial region is largely composed of a thick layer of transversely oriented collagen fibers intermixed with elastic fibers and glycosaminoglycans.[21,22]

The effect on scaffold architecture and changes in molecular composition due to these aggressive decellularizing agents is likely to alter cell interactions, and thus the phenotypic response that cells have towards the scaffolds will also vary.[23–25] As such, in conjunction with our analysis of the effect on decellularization on mass transfer, the effects on cell migration, metabolism, and proliferation were also assessed.

MATERIALS AND METHODS

HUV isolation

HUVs were isolated from placentas collected at Shands Hospital at the University of Florida (Gainesville, FL) using an automated dissection method as previously described.[15] Briefly, 100 mm segments of 1-day-old human umbilical cords were collected and mounted onto stainless steel mandrels and frozen to −80°C overnight. Frozen vessels were then loaded into a 10″ CNC bench lathe (MicroKinetics, Kennesaw, GA), and cut to the desired thickness (below) at a rotational speed of 2800 RPM with an axial cutting rate of 5 mm/s. Samples were lathed to create 750 μm thick (full thickness) and 250 μm thick (intima and proximate-media region) scaffolds. For samples needing the intimal region removed, the veins were inverted so the lumenal side was facing out, then re-lathed, under the same procedure described above. This removed the basement membrane by dissecting away 250 μm from the lumenal wall (Fig. 1). Finally, freshly lathed cords were placed in a fridge at 5°C for 4 h before decellularization.

Decellularization

Dissected HUV samples were placed into 100 mL KIMAX media storage bottles along with a primary solvent to obtain a solvent/tissue mass of 20:1 (w:v). Phosphate buffered saline (PBS) at a pH 7.4 was used for all necessary steps in the decellularization process. The three individual primary solvents were: (1) 1% SDS (Thermo Scientific, Rockford, IL) solution diluted into PBS, (2) 1% TX100 (Thermo Scientific, Rockford, IL) solution diluted into PBS, and (3) a 20:80 ACE/EtOH (Fisher Scientific, Waltham, MA) Solution. Dissected tissue sections were placed on an orbital shaker plate at 100 rpm for 24 h. Samples were then washed with PBS at 30 min, 1, 3, 6, 12, and 24 h. Samples were incubated overnight at 37°C in a 70 U/mL DNase I solution (Sigma-Aldrich, St. Louis, MO) in PBS. Next, they were rinsed in PBS at 1, 6, 12, and 24 h. Finally, samples were sterilized using a 0.2% peracetic acid/4% ethanol (Sigma- Aldrich, St. Louis, MO) solution for 2 h and then pH balanced (7.4) using multiple washes of PBS.

Determination of molecular mass flux rates and effective diffusion coefficients using BSA

Mass flux rates were measured using albumin stained with Coomossie Brilliant Blue G-250 as a traceable marker over the experimental time course. A two-chambered isolation setup was used with the HUV scaffold acting as a permeable membrane between the two chambers. Chamber 1 contained 250 mL of a 2 mg/mL solution of bovine serum albumin (BSA; Sigma-Aldrich, St. Louis, MO) in PBS solution, and chamber 2 contained 250 mL of PBS (Fig. 2). For the first 2 weeks, 1 mL of solution was taken daily from chamber 2, and then buffer solution in chamber 2 was changed with fresh PBS. During the remainder of the experimental period, samples were taken and buffers were changed every 3 days.

Mass flux of the BSA protein was calculated by quantifying the formation of the protein-Coomassie G250 dye-complex (Thermo Scientific, Rockford, IL), as per manufactures instructions. Briefly, 150 μL of Bradford reagent was added to each of the sample solutions, and then incubated at 25°C for 10 min. The protein-dye complex was measured at 595 nm using a Synergy II microplate reader (BioTek, Winooski, VT). Albumin mass flux rates were calculated as the average grams of albumin diffused into chamber 2 over 24 h, and measurements were taken over a period of 28 days. Diffusion coefficients are included to extrapolate the relationship between mass flux and tissue thickness. The effective diffusion coefficients ($D_{\text{effective}}$) were calculated as $D^* \varphi$ for each day based on the assumption of quasi-steady transport across the membrane[26]:

$$D=\varphi=\ln\left(\frac{2C_2 - C_1}{C_1}\right)\frac{VL}{2A_m t} \quad (1)$$

where D is the diffusion of albumin in tissue and φ is the partition coefficient. V is the chamber volume ($V = V1 = V2$), tissue thickness (L), cross-sectional area of the membrane (A_m), time ($t = 24$ h), the initial concentration on the albumin containing side (C_1), and the concentration in $V2$ after time t (C_2). The partition coefficient is equal to the ratio of the concentration of albumin in the tissue to the concentration of albumin in the equilibrated solution.[27] Among samples, we assume a negligible difference for the ratio of the albumin concentration in the tissue to the concentration of albumin in the equilibrated solution, therefore, φ is approximately equivalent for all samples. Thus, even though φ is not determined, the lumped parameter $D^* \varphi$ allows a relatively accurate comparison of albumin diffusion trends among the samples. Mass flux and $D_{\text{effective}}$ were calculated using data collected after mass flow rate reached steady state.

Albumin degradation was assessed over 7 days to ensure that decellularized samples did not contain metalloproteinases or residual decellularization solution that may interfere with the BSA assay. Known quantities of albumin were mixed in PBS with the decellularized HUV, and assays were performed daily to ensure no decrease (or increase) in absorbance reading due to unknown molecular interferences. The effect of multiple freezes on scaffold architecture (which is part of the lathing procedure described above) was assessed to verify that it did not significantly affect molecular diffusion. To assess the effects of freezing, scaffolds were processed through one, two, or three freeze thaw cycles going from 25 to −85°C over a 12 h period. No significant differences occurred between the one, two, and three freeze/thaw cycle groups with respect to BSA diffusion rate, data not shown. Diffusion in nonprocessed tissues was negligible (zero values) over 28 days (data not shown), as such data is presented as a direct comparison of the three decellularization methods.

Determination of O_2, glucose, and K^+ diffusion rates

Using the same isolation chambers containing a total solution volume of 250 mL (Fig. 2), a BioProfile 400 Nutrient Analyzer, (Nova Biomedical, Waltham, MA) was used to analyze 1

mL aliquots at appropriate time intervals. For sampling oxygen diffusion rates each chamber was filled with 1% FBS (Gibco, Carlsbad, CA) supplemented low-glucose DMEM (HyClone, Rockford, IL). Then, one of the airtight chambers was equilibrated to 1% oxygen while the other was equilibrated to 21% oxygen. After 24 h of exposure to each respective oxygen condition, creating an oxygen gradient across the tissue, the chamber exposed to 1% Oxygen was closed (airtight) so that oxygen could diffuse from the other chamber through the HUV sample. For sampling of glucose and potassium diffusion rates, 1% FBS supplemented low-glucose DMEM was put into one chamber while PBS was put into the other chamber (to create a gradient). The amount of glucose, potassium, and oxygen was recorded in grams per liter, milimoles per liter, and moles per hour, respectively.

Histology

Standard hematoxylin (Richard-Alan Scientific, Kalamazoo, MI) and eosin (Richard-Alan Scientific, Kalamazoo, MI; H&E) staining was used for histology. Samples were cut into 10 mm by 10 mm squares from our tubular decellularized scaffolds. After experiment termination, tissue samples were embedded in Neg-50 frozen section medium and then sectioned into 5 μm sections using a Microm HM550 cryostat (Thermo Scientific, Waltham, MA). Sections were fixed, stained, and dehydrated, and then images were captured using an Imager M2 light microscope (Zeiss, Oberkochen, Germany) with a Axiocam HRm digital camera (Zeiss, Oberkochen, Germany).

Cell culture and seeding

Decellularized HUV sections were immersed in 10% FBS (Gibco, Carlsbad, CA) supplemented low-glucose DMEM (HyClone, Rockford, IL). Human smooth muscle cells, CRL-1999, were used between passages 5 and 10 (ATCC, Manasses, VA) and cultured under standard conditions at 37°C and 5% CO_2. Cells were detached from cell culture plates using Accutase (Thermo Scientific, Waltham, MA), centrifuged, then the cell pellet was resuspended in media, and 2 mL of the 500,000 cell/mL solution was pipetted onto each presoaked 10 mm by 10 mm tissue sample.[28,29] Samples were incubated for 10 days, and cell culture media was changed every other day.

Cell proliferation and metabolism

Immediately at the conclusion of experimentation, samples were cut into two halves. One-half was frozen for cryosectioning and histology, and the other half was used immediately for analysis of cell metabolism and proliferation. Samples were weighed then cell metabolism was quantified using an AlamarBlue (AB) reduction assay (Invitrogen, Carlsbad, CA), according to manufactures instructions. Final values were given as the percent reduction (AB) per gram of tissue for each sample. Following this nondestructive cellular assay, DNA per gram of tissue was quantified using the PicoGreen (Invitrogen, Carlsbad, CA) assay as per manufactures instructions. Assuming an average of 6 pg DNA per cell (determined experimentally), results were represented as cells per milligram tissue.

Cell migration

Cell migration data was collected using sections from H&E histology in conjunction with computer analysis. Sections of 5 × 5 μm from each tissue sample were collected with a distance of 20 μm between each consecutive slice and stained with H&E. Images of each section were analyzed for cell migration using ImageJ (NIH, Bethesda, MD) by quantifying the shortest distance of migration from the seeded ablumenal surface to the center of each cell (all visible cells) and then averaged to obtain the average distance of cell migration at a magnification of 5× using a light microscope (Zeiss, Axio Imager M2, Germany).

Statistics

Results are reported as mean ± standard deviation. Data analysis was performed using SPSS (IBM, Somers, NY). To determine differences between time points for each sample-type, a one-way analysis of variance (ANOVA) or a nonparametric ANOVA (Kruskal-Wallis Test) was performed to determine statistical significance ($p < 0.05$) within each data set. When the analysis of variance detected significance, a Tukey's Multiple Comparison Test (one-way ANOVA) or a Dunn's Multiple Comparison Test (Kruskal-Wallis Test) was used at a 95% confidence level. To determine differences between different sample-types at the two time points, we performed a *t*-test or a Mann-Whitney Rank Sum Test to determine statistical significance ($p < 0.05$). While $n = 3$ is a small sample size, the low standard deviations and narrow data ranges gives confidence in the results.

RESULTS

Histology

Hematoxylin and eosin staining of differentially decellularized scaffolds show significant differences in morphology throughout all regions of the scaffold (Fig. 3). SDS treated tissue samples had more clumped collagen fibers in the intima, relative to either TX100 or ACE/EtOH decellularization. ACE/EtOH decellularization produced the most visible modification of the native scaffold, with the intimal, medial, and the ablumenal zones all displaying clumped collagen fibers. Qualitatively, the SDS decellularization treatment led to the second most harshly altered scaffold morphology. While the intimal region appeared largely intact, the medial and adventitial regions had clumped collagen fibers; however, the degree of collagen fiber clumping was much less than that of the ACE/EtOH decellularized samples. Finally, TX100 samples appeared to have a morphology almost unaltered from the native tissue, although a negligible amount of clumped collagen fibers were visible.

BSA diffusion through regions

The mass flux of albumin through tested HUVs was constant after the first 2 days with a minor burst effect exhibited in the preceding days. This trend is observed in Figures 4–6 in which the percent albumin transported across the membrane has an approximately constant slope after the burst effect, which occurs during the first few days. The intima and proximate media region was shown to be the primary mass transfer limitation of albumin irrespective of decellularization method as seen by comparing the effective diffusion coefficient in the MAR $1.16 \times 10^{-6} \pm 0.06 \times 10^{-6}$ cm^2/s with that in the IMR at $0.64 \times 10^{-6} \pm 0.15 \times 10^{-6}$ cm^2/s (Table I).

Choice of decellularization method had variable effects on each of the dissected regions. For example, in the MAR and the FTR regions, no differences were seen in the mass flux of BSA with respect to each of the three-decellularization methods (Table I). However, in the IMR the mass flux varies depending on decellularization method. Specifically, the BSA mass flux rate increases from 7.80 ± 0.47 to 9.75 ± 2.82 μg/h with the SDS and TX100 samples to 15.20 ± 2.66 μg/h in the ACE/EtOH samples (Table I). At 14 days, a noticeable change in mass flux (slope) occurs because, as detailed in the methods section, the osmotic gradient was reset daily during the first 2 weeks, but every third day subsequently (Figs. 4–6).

Oxygen, glucose, and potassium flux

Studies of oxygen, glucose, and potassium flux rates, showed that decellularization technique affects the diffusion kinetics of molecules on a predominantly individual basis. Oxygen was found to diffuse fastest through ACE/EtOH decellularized samples, at a rate of

0.0006 mol/h, whereas the rate was 0.0003 and 0.0002 mol/h in the TX100 and SDS samples, respectively (Fig. 7).

Glucose flux followed a similar trend displaying increased diffusion across the ACE/EtOH samples relative to the TX100 samples, specifically 2 g/L/h more. No difference was seen between SDS and the other sample groups. Overall, glucose flux was affected by the specific decellularization process (Fig. 8). Finally, no difference in the potassium flux rate was noted between the three-decellularization sample groups (Fig. 9).

Cell seeded scaffolds

Cell migration and proliferation studies showed that HUVs decellularized with TX100 had the most cell migration. After 10 days, the migration in 1% SDS decellularized samples was 46% less than that of the TX100 samples, with migration distances from the albumen of 61 ± 22 μm (Fig. 10). Migration in SDS samples after 10 days was 27 ± 14 and 42 ± 11 μm in ACE/EtOH samples.

Metabolic activity in the TX100 decellularized samples was significantly greater than in the ACE/EtOH samples despite having less cells per gram of tissue when compared with the ACE/EtOH decellularized samples (Fig. 10). The lowest metabolic activity among sample groups was 44 ± 10% reduction of AB per gram tissue, whereas the highest rate was 64 ± 14% reduction of AB per gram tissue with TX100. The amount of cells per milligram tissue was highest in ACE/EtOH samples, at 4.33 ± 0.50 million cells/mg tissue, and lowest in SDS samples, at 3.00 ± 0.33 million cells/mg tissue.

DISCUSSION

Specificities of the decellularization chemistry have significant effects on the scaffold molecular architecture that result in variable effects on mass transfer and cellular response. While decellularization affects both mass transfer and cellular response, it does not do so in an easily predictable manner. Although some decellularization protocols encourage the cellular migration response, they decrease the overall mass transfer properties. For example, histological analysis showed that treatment using ACE/EtOH to decellularize the tissue resulted in collagen fibers displaying a more clumped morphology in the intimal region, relative to either TX100 or ACE/EtOH decellularization treatments. The clumping of collagen, which occurs in the tightly woven intimal layer of the ACE/EtOH decellularized samples, leads to higher porosity and higher mass flux rates. However, ACE/EtOH decellularized scaffolds also had low cell migration and metabolic activity when compared with TX100 decellularized samples, confirming that nutrient transfer is only one of many parameters that modulate cell function.

While the overall mass flux rates of albumin through each zone (IMR, MAR, and FTR) were similar, these regions display significant differences in the effective diffusion coefficient where the tightly woven IMR region is the primary limitation to mass transfer irrespective of decellularization method. The significance of these regional variations in scaffold architecture is the location of the diffusion limiting zone relative to the nutrient source, where cells in regions distal to the nutrient source will be more nutrient deprived. Similarly, the FTR region had an overall mass flux rate similar to the individual dissected components; however, the region had a higher effective diffusion coefficient than either the IMR or MAR. The hypothesis is that this is due to variation in the layer structure between the dissected component layers, where changes to the tissue architecture that result from decellularization may be dependent on how surrounding tissue structures affect the final architecture. In other words, the two zones of the FTR may have provided structural support

for one another during the decellularization process, which was not present in the dissected component regions.

Creation of a uniformly cell dense scaffold is important in many tissue engineering applications. These studies have also shown that due to the heterogeneous structure and composition of *ex vivo* materials, regional variations in mass transport occur in a manner that is dependent on the decellularization protocol. When decellularizing a tissue, consideration must be made about how a solution can affect two separate zones of a single scaffold differently; for example, a decellularization solution might cause more architectural changes to an intimal region, with type IV collagen, relative to a medial region, with more collagen type III. Thus, optimizing the decellularization method to create the least regional variations can aid in the formation of uniformly cell dense scaffolds. These investigations have shown that different decellularization methods affect the mass flux in direct relation to the treatment chemistry and the specified nutrient. This is more obvious in the IMR region where albumin mass flux rates vary significantly as a function of the decellularization method. This is an important consideration if the limiting nutrient of a developing construct can be identified, so that the initial decellularization techniques can be tailored to the material of choice.

Analysis of oxygen, glucose, and potassium flux rates also reveals the complex nature of these transport conditions as a function of decellularization method. Oxygen diffusion was found to be the fastest through the ACE/EtOH samples, having an average flux rate that was three times faster than in SDS decellularized samples and two times faster than TX100 decellularized samples. Increased oxygen flux though the ACE/EtOH samples correspond to increased albumin diffusion through the intimal/proximate medial regions.

As a positively charged small molecule, it is interesting that no difference is noted in potassium flux rates among sample groups. While differences are seen in the flux rates of negatively charged oxygen, the lack of differences in the flux rate of this positively charged molecule can likely be attributed to either its higher solubility in cell culture media or its positive charge and charge effects within the ECM. Scaffold charge effects would also be imparted by residual SDS, which was not removed during the decellularization wash steps resulting in a net negative charge; likewise, TX100 have no charge and would not alter the overall charge on scaffold surfaces.

In addition to modifying scaffold architecture, the decellularization solvents and surfactants also led to changes in the cellular response. These changes were caused by the variable modification of the native ECM molecules that was dependent on the specific decellularization solution. These investigations show that samples decellularized with TX100 promoted the farthest cell migration and the highest metabolic activity by comparison to either ACE/EtOH or SDS decellularized samples. However, cells seeded on TX100 samples did not have the highest cell densities relative to other treatments. The high migration and metabolic activity in conjunction with the low cell density with TX100 samples indicates that the phenotype of cells seeded onto these scaffolds became more metabolically active yet less proliferative when compared to cells cultured on either SDS or ACE/EtOH treated samples. Scaffolds with the slowest recellularization response were decellularized with SDS, based on reduced cell migration and cell density. Interestingly, by comparison to the other methods tested, SDS decellularization resulted in improved retention of the native HUVs scaffold architecture as seen by mass flux rates, effective diffusion coefficient values, and histological analysis, even though it displayed suboptimal cell responses. Despite the expected cellular benefits of a scaffold, which retains more of its native molecular architecture, these suboptimal cell responses noted with SDS treated

constructs could be caused by residual SDS or changes in surface chemistry caused during decellularization.[30]

The significance of mass transfer is important initially for cell migration and then during maturation as cellular phenotypes revert, ideally to a more quiescent state with restored functionality. The rate at which a scaffold remodels will vary based on the rate of cell migration, and this rate will in part be regulated by the transport conditions within the scaffold. It is also important that a scaffold regenerate rapidly particularly when exposed to constant physiological stress or biologically sensitive conditions that may result in overt scaffold degradation or failure. As such, poor transport conditions will result in slower migration and proliferation rates that ultimately increase the probability of graft failure. These results have shown that the regional mass transfer variation that occurs with respect to each decellularization method could cause the recellularization response to occur at different rates from one region to another. Where the IMR shows improved transport conditions when decellularized with ACE/EtOH relative to decellularization with TX100 and SDS, the MAR shows no improvement when comparing each of the three-decellularization methods.

Creation of an effective vasculature network in *ex vivo* materials can be aided by selective decellularization to optimize mass transfer and cellular integration characteristics; however, the creation of an effective vasculature remains the primary goal to support effectively cell dense materials. With the different approaches taken to decellularize *ex vivo* materials, it is clear that these processes have a significant impact not only on cell removal but also on ECM architecture, which in turn affects transport conditions and cell function. Further investigation is required to understand the molecular mechanisms that drive differential cell function in order to produce clinically functional materials.

Acknowledgments

The authors would like to thank Alan Miles for fabrication of the diffusion chambers.

Contract grant sponsor: National Institute of Health; contract grant number: NIH R01 HL088207

REFERENCES

1. Gilbert TW, Sellaro TL, Badylak SF. Decellularization of tissues and organs. Biomaterials. 2006; 27:3675–3683. [PubMed: 16519932]
2. Rieder E. Decellularization protocols of porcine heart valves differ importantly in efficiency of cell removal and susceptibility of the matrix to recellularization with human vascular cells. J Thorac Cardiovasc Surg. 2004; 127:6.
3. Chung CA, Yang CW, Chen CW. Analysis of cell growth and diffusion in a scaffold for cartilage tissue engineering. Biotechnol Bioeng. 2006; 94:1138–1146. [PubMed: 16586509]
4. Williams C, Liao J, Joyce EM, Wang B, Leach JB, Sacks MS, Wong JY. Altered structural and mechanical properties in decellularized rabbit carotid arteries. Acta Biomater. 2009; 5:993–1005. [PubMed: 19135421]
5. Liao J, Joyce EM, Sacks MS. Effects of decellularization on the mechanical and structural properties of the porcine aortic valve leaflet. Biomaterials. 2008; 29:1065–1074. [PubMed: 18096223]
6. Martin Y, Vermette P. Bioreactors for tissue mass culture: Design, characterization, and recent advances. Biomaterials. 2005; 26:7481–7503. [PubMed: 16023202]
7. Duan X, McLaughlin C, Griffith M, Sheardown H. Biofunctionalization of collagen for improved biological response: Scaffolds for corneal tissue engineering. Biomaterials. 2007; 28:78–88. [PubMed: 16962168]

8. Gibbons GH, Pratt RE, Dzau VJ. Vascular smooth muscle cell hypertrophy vs hyperplasia. Autocrine transforming growth factor-beta 1 expression determines growth response to angiotensin II. J Clin Invest. 1992; 90:456–461. [PubMed: 1644917]
9. Whang K, Healy KE, Elenz DR, Nam EK, Tsai DC, Thomas CH, Nuber GW, Glorieux FH, Travers R, Sprague SM. Engineering bone regeneration with bioabsorbable scaffolds with novel micro-architecture. Tissue Eng. 1999; 5:35–51. [PubMed: 10207188]
10. Hubbell JA. Biomaterials in tissue engineering. Biotechnology (N Y). 1995; 13:565–576. [PubMed: 9634795]
11. Malda J, Woodfield TB, van der Vloodt F, Kooy FK, Martens DE, Tramper J, van Blitterswijk CA, Riesle J. The effect of PEGT/PBT scaffold architecture on oxygen gradients in tissue engineered cartilaginous constructs. Biomaterials. 2004; 25:5773–5780. [PubMed: 15147823]
12. Schittny JC, Yurchenco PD. Basement membranes: Molecular organization and function in development and disease. Curr Opin Cell Biol. 1989; 1:983–988. [PubMed: 2697299]
13. Yurchenco PD, Schittny JC. Molecular architecture of basement membranes. FASEB J. 1990; 4:1577–1590. [PubMed: 2180767]
14. Li WC, Zhang HM, Wang PJ, Xi GM, Wang HQ, Chen Y, Deng ZH, Zhang ZH, Huang TZ. Quantitative analysis of the microstructure of human umbilical vein for assessing feasibility as vessel substitute. Ann Vasc Surg. 2008; 22:417–424. [PubMed: 18466819]
15. Daniel J, Abe K, McFetridge PS. Development of the human umbilical vein scaffold for cardiovascular tissue engineering applications. ASAIO J. 2005; 51:252–261. [PubMed: 15968956]
16. Cartmell JS, Dunn MG. Effect of chemical treatments on tendon cellularity and mechanical properties. J Biomed Mater Res. 2000; 49:134–140. [PubMed: 10559756]
17. Lumpkins SB, Pierre N, McFetridge PS. A mechanical evaluation of three decellularization methods in the design of a xenogeneic scaffold for tissue engineering the temporomandibular joint disc. Acta Biomater. 2008; 4:808–816. [PubMed: 18314000]
18. Montoya CV, McFetridge PS. Preparation of ex vivo-based biomaterials using convective flow decellularization. Tissue Eng Part C Methods. 2009; 15:191–200. [PubMed: 19196128]
19. Woodley DT, Rao CN, Hassell JR, Liotta LA, Martin GR, Kleinman HK. Interactions of basement membrane components. Biochim Biophys Acta. 1983; 761:278–283. [PubMed: 6228259]
20. Bankowski E, Sobolewski K, Romanowicz L, Chyczewski L, Jaworski S. Collagen and glycosaminoglycans of Wharton's jelly and their alterations in EPH-gestosis. Eur J Obstet Gynecol Reprod Biol. 1996; 66:109–117. [PubMed: 8735730]
21. Pauly RR, Passaniti A, Bilato C, Monticone R, Cheng L, Papadopoulos N, Gluzband YA, Smith L, Weinstein C, Lakatta EG. Migration of cultured vascular smooth muscle cells through a basement membrane barrier requires type IV collagenase activity and is inhibited by cellular differentiation. Circ Res. 1994; 75:41–54. [PubMed: 8013081]
22. Lethias C, Labourdette L, Willems R, Comte J, Herbage D. Composition and organization of the extracellular matrix of vein walls: Collagen networks. Int Angiol. 1996; 15:104–113. [PubMed: 8803633]
23. Meyer SR, Nagendran J, Desai LS, Rayat GR, Churchill TA, Anderson CC, Rajotte RV, Lakey JR, Ross DB. Decellularization reduces the immune response to aortic valve allografts in the rat. J Thorac Cardiovasc Surg. 2005; 130:469–476. [PubMed: 16077415]
24. Bertipaglia B, Ortolani F, Petrelli L, Gerosa G, Spina M, Pauletto P, Casarotto D, Marchini M, Sartore S. Cell characterization of porcine aortic valve and decellularized leaflets repopulated with aortic valve interstitial cells: The VESALIO Project (Vitalitate Exornatum Succedaneum Aorticum Labore Ingenioso Obtenibitur). Ann Thorac Surg. 2003; 75:1274–1282. [PubMed: 12683575]
25. Ariganello MB, Simionescu DT, Labow RS, Lee JM. Macrophage differentiation and polarization on a decellularized pericardial biomaterial. Biomaterials. 2011; 32:439–449. [PubMed: 20933269]
26. Truskey, GA.; Yuan, F.; Katz, DF. Transport phenomena in biological systems. Upper Saddle River (NJ): Pearson Prentice Hall; 2009.
27. Anderson OA, Jackson TL, Singh JK, Hussain AA, Marshall J. Human transscleral albumin permeability and the effect of topographical location and donor age. Invest Ophthalmol Vis Sci. 2008; 49:4041–4045. [PubMed: 18450593]

28. Seifalian AM, Tiwari A, Hamilton G, Salacinski HJ. Improving the clinical patency of prosthetic vascular and coronary bypass grafts: The role of seeding and tissue engineering. Artif Organs. 2002; 26:307–320. [PubMed: 11952502]

29. McFetridge PS, Bodamyali T, Horrocks M, Chaudhuri JB. Endothelial and smooth muscle cell seeding onto processed ex vivo arterial scaffolds using 3D vascular bioreactors. ASAIO J. 2004; 50:591–600. [PubMed: 15672794]

30. Gratzer PF, Harrison RD, Woods T. Matrix alteration and not residual sodium dodecyl sulfate cytotoxicity affects the cellular repopulation of a decellularized matrix. Tissue Eng. 2006; 12:2975–2983. [PubMed: 17518665]

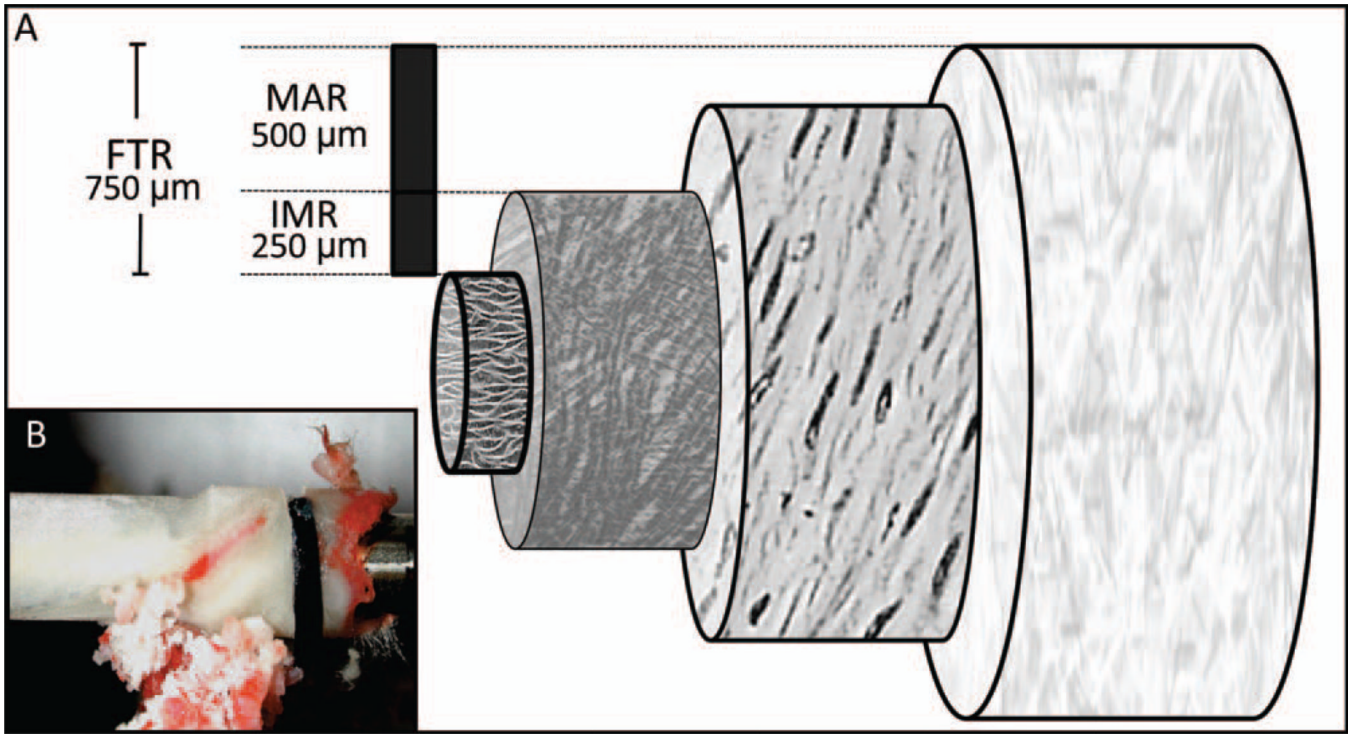

FIGURE 1.

Representative HUV demarcated with dissection zones and HUV in process of dissection. A: The native HUV was dissected into three different architectural regions including the intima and proximate-media region (IMR), the medial/adventitial region (MAR), and the full tissue region (FTR). The thickness of the FTR was 750 μm, while the thickness of the MAR and IMR was 500 and 250 μm, respectively. B: The zones were dissected using an HUV mounted onto a mandrel. [Color figure can be viewed in the online issue, which is available at wileyonlinelibrary.com.]

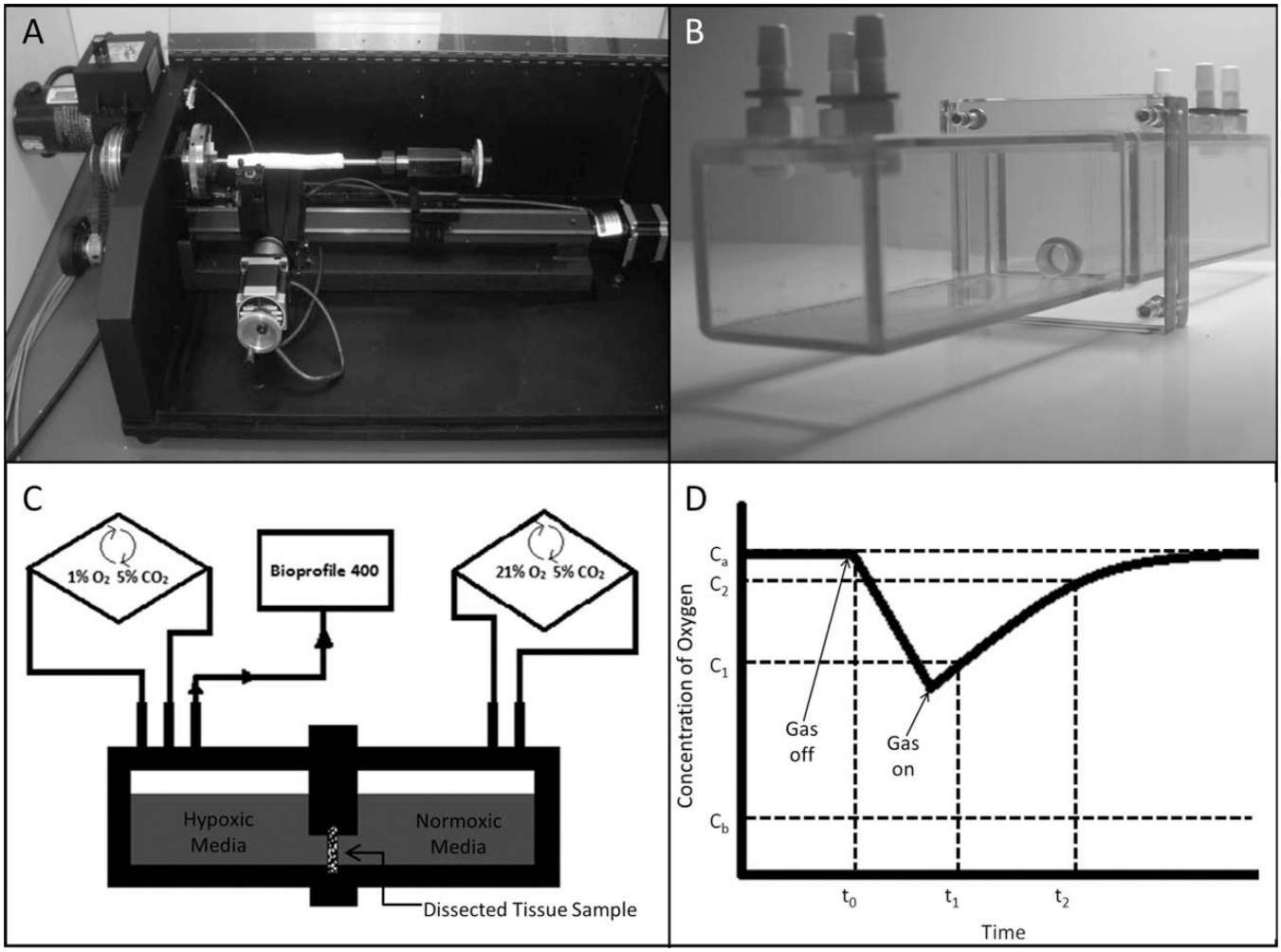

FIGURE 2.

A: Computer numerical controlled (CNC) dissection lathe, (B) diffusion chamber and (C) setup-schematic, and (D) representative oxygen diffusion rate graph. To determine the average gas flux values through the tissue, the air in one chamber was turned from the off to the on position, and then the time to reach the atmospheric air concentrations was measured in the other chamber.

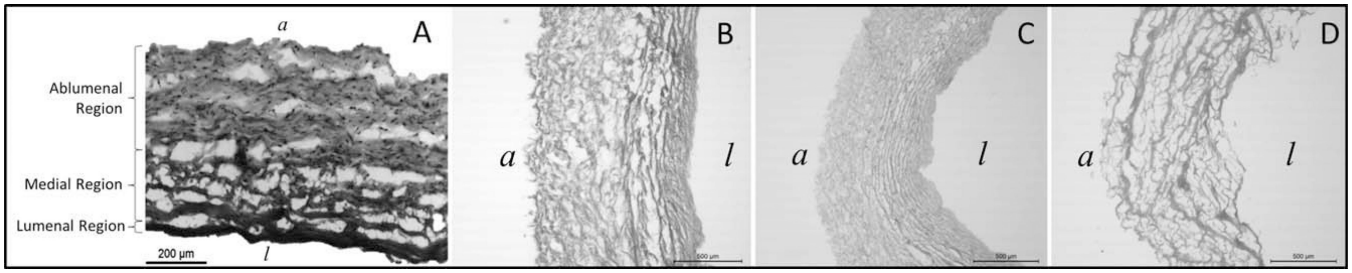

FIGURE 3.

Representative H&E Histology of native and acellular HUVs. H&E stained samples of the HUV were lathed to 750 μm thicknesses. The (A) native HUV is shown in addition to samples decellularized with (B) 1% SDS solution, (C) 1% Triton X-100 solution, and (D) ACE/EtOH solution. Tissue orientation is indicated with a "*l*" for the lumenal side and an "*a*" for the ablumenal side. $n = 3$ for each decellularization method.

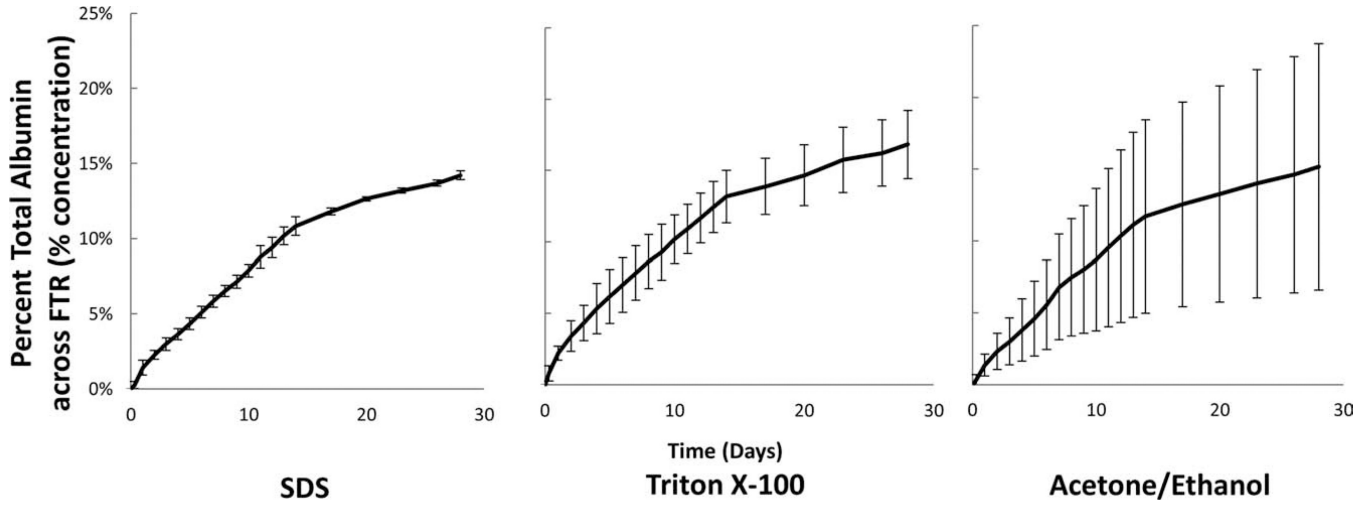

FIGURE 4.

Percent total albumin calculated as the percent from reservoir V1 transported across the FTR. The mass flux of albumin across full thickness (750 μm) vessels was the same among decellularization methods. $n = 3$ for each decellularization method.

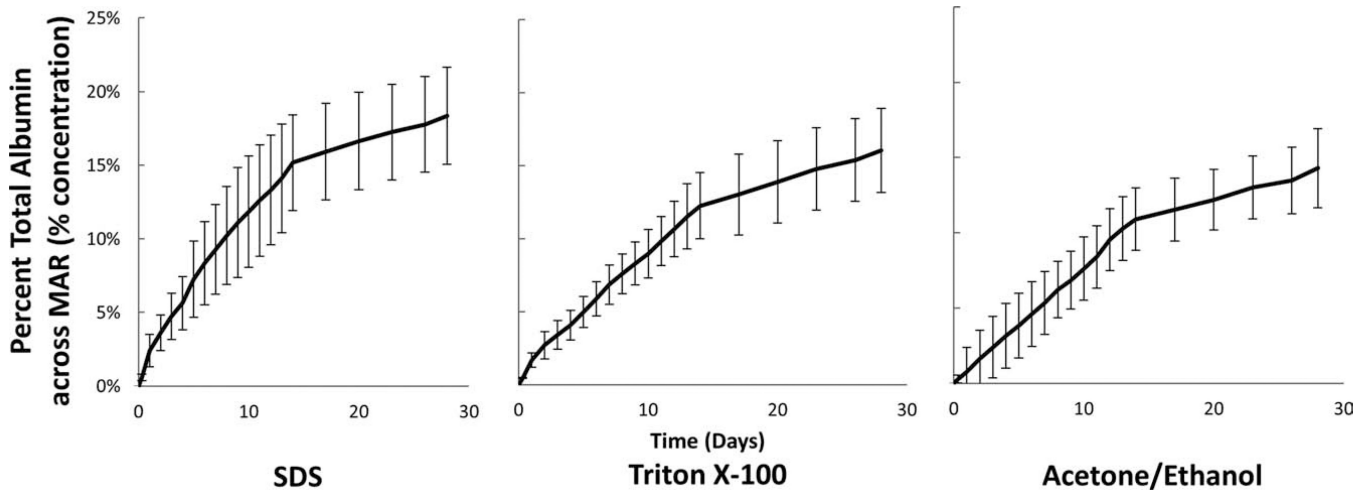

FIGURE 5.

Percent total albumin calculated as the percent from reservoir V1 transported across the MAR. The mass flux of albumin across the medial/adventitial region of (500 μm) vessels was the same among decellularization methods. $n = 3$ for each decellularization method.

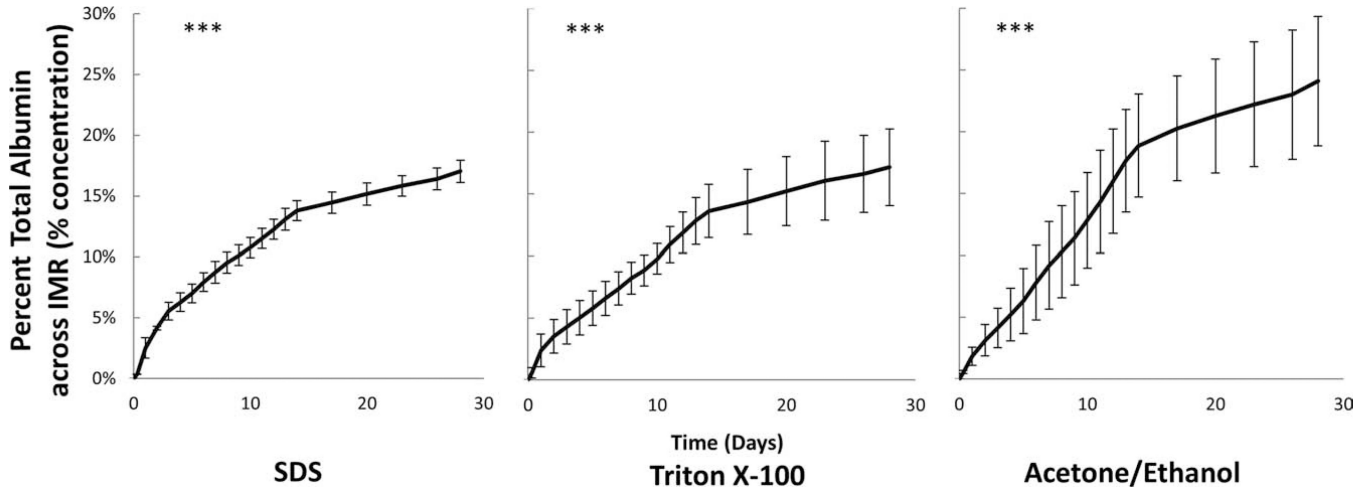

FIGURE 6.

Percent total albumin calculated as the percent from reservoir V1 transported across the IMR. The mass flux of albumin across the intimal and proximate-media region (<250 μm) was greatest among ACE/EtOH decellularized samples. ***Indicates $p < 0.001$ between groups. $n = 3$ for each decellularization method.

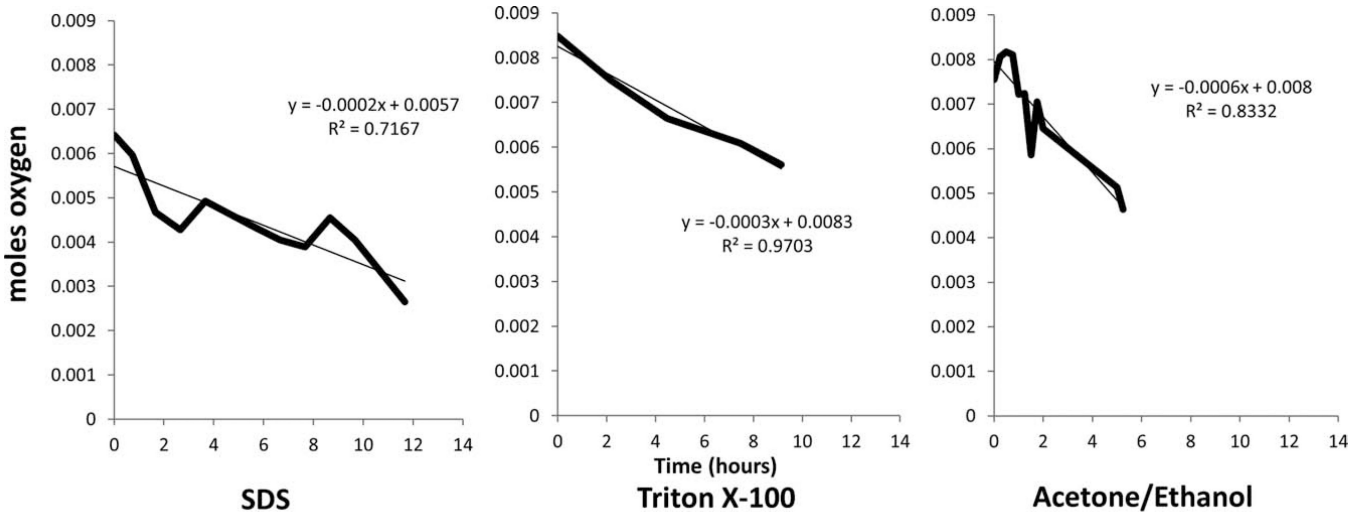

FIGURE 7.

Oxygen flux across the FTR region with respect to decellularization solution. Flux of oxygen was through the full thickness HUV samples decellularized with SDS, Triton X-100, and ACE/EtOH. For each given decellularization method, the data presented is the average of three experiments ($n = 3$).

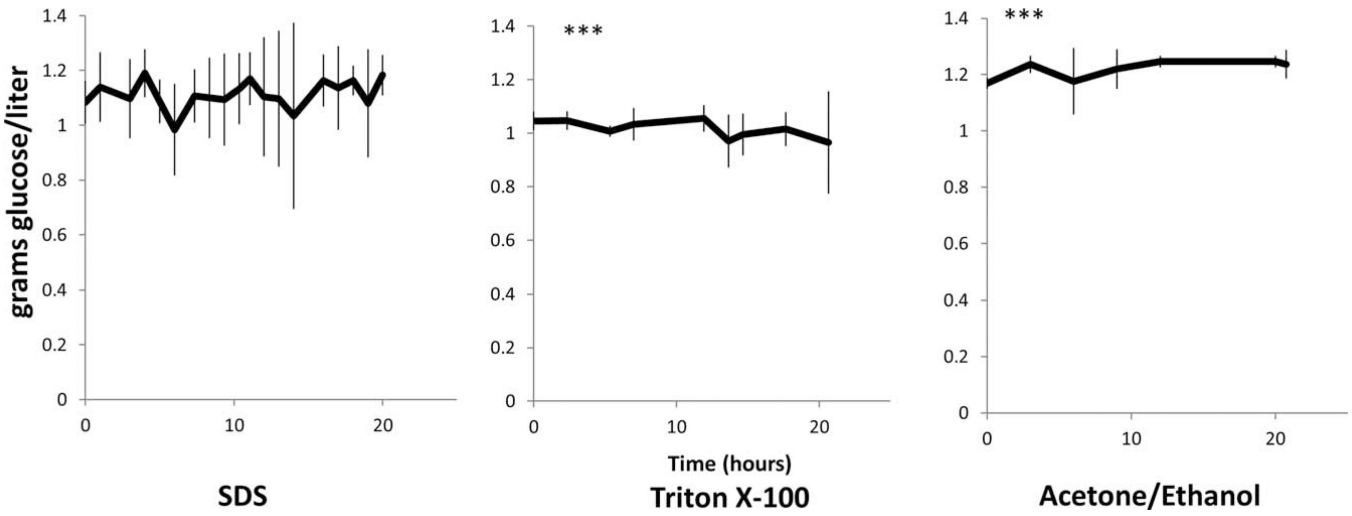

FIGURE 8.

Glucose mass flux across the FTR region with respect to decellularization solution. Mass flux rate of glucose was through the full thickness HUV decellularized with SDS, Triton X-100, and ACE/EtOH. $n = 3$ for each decellularization method. Between Tx-100 and Ac/Et sample, $p = 0.01$ at a 95% confidence level.

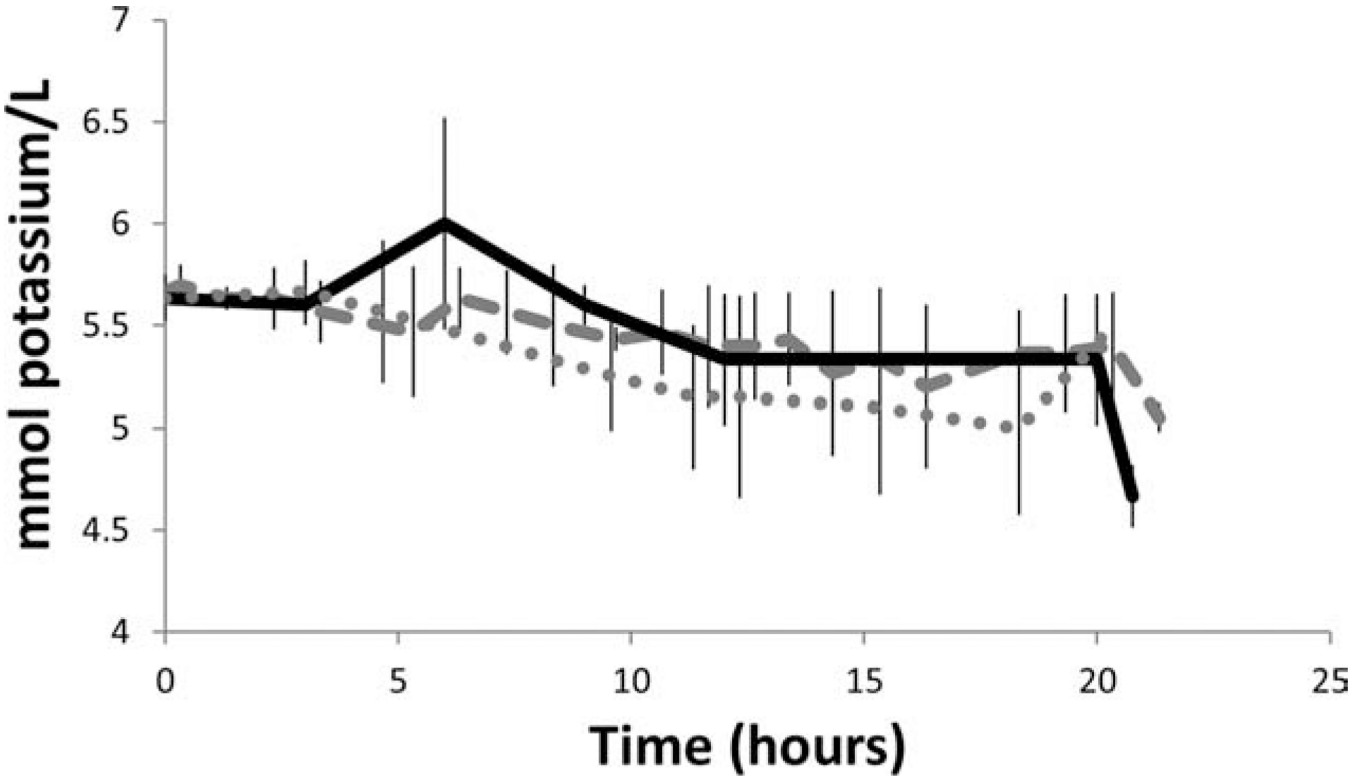

FIGURE 9.

Potassium flux across the FTR region with respect to decellularization solution. Flux of potassium was through the full thickness HUV decellularized with SDS (dashed), Triton X-100 (dotted), and ACE/EtOH (solid); $n = 3$.

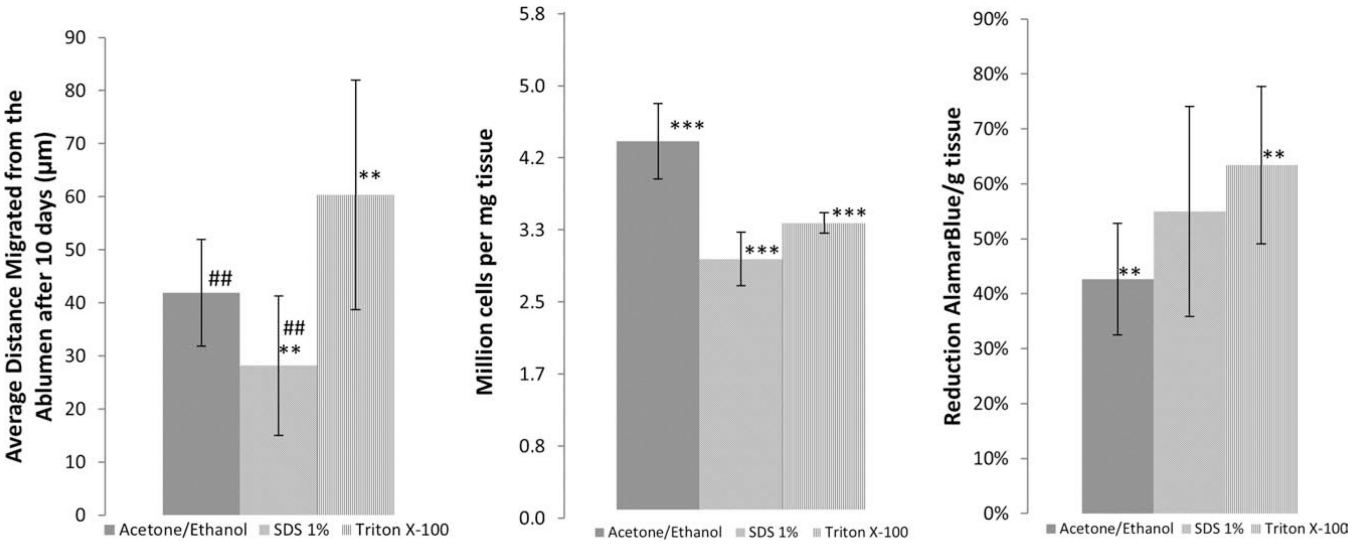

FIGURE 10.

Cell migration, proliferation, and metabolic activity. Average distances migrated from the ablumen after 10 days. To determine metabolic activity, the percent reduction of AlamarBlue per gram of tissue was calculated and to determine the amount of DNA per mg tissue a Pico Green Assay was used. One-Way ANOVA was used to determine statistical significance, when the analysis of variance detected significance, a Tukey's multiple comparison test (one-way ANOVA) or a Dunn's multiple comparison test (Kruskal-Wallis Test) was run with a confidence level of 95%. Between SDS and TX100 samples $p = 0.0168$ and between ACE/EtOH and SDS $p = 0.025$; $n = 3$.

TABLE I

Average Albumin Mass Flux Rate and Effective Diffusion Coefficient by Region and Decellularization Method

Sample Region	Decellularization Method	Mass Flux (μg/h)	Effective Diffusion Coefficient ($D_{eff} \times 10^{-6}$ cm^2/s)
Intimal and Proximate-Media	SDS	7.80 ± 0.47[b]	0.53 ± 0.31
Region (IMR)[a] 250 μm thickness	TX100	9.75 ± 2.81[b]	0.60 ± 0.29
	Et/Ac	15.20 ± 2.65[b]	0.81 ± 0.35
Media/Adventitial Region (MAR)[a]	SDS	8.91 ± 1.95	1.22 ± 0.19
500 μm thickness	TX100	8.52 ± 1.96	1.12 ± 0.49
	Et/Ac	8.70 ± 0.63	1.13 ± 0.57
Full Thickness Region (FTR)[a]	SDS	7.83 ± 0.73	1.51 ± 0.67
750 μm thickness	TX100	8.34 ± 0.21	1.75 ± 0.83
	Et/Ac	8.05 ± 0.38	1.63 ± 0.80

Average mass flux rate for all decellularization sample types are represented as mean mg albumin per h ± std dev.

[a] $p < 0.001$ when comparing between the FTR, IMR, and MAR mass flux data and effective diffusion coefficient values, respectively. Analysis was performed using a one-way ANOVA at 95% confidence level. $n = 3$ for each sample type.

[b] A statistical significance of mass flux rate of $p \leq 0.017$ among samples types within the same region.